Energy 152 (2018) 313–321

Contents lists available at ScienceDirect

Energy

journal homepage: www.elsevier.com/locate/energy

Control optimization to achieve energy-efficient operation of the air separation unit in oxy-fuel combustion power plants

Bo Jin [a, b], Haibo Zhao [a, *], Chuguang Zheng [a], Zhiwu Liang [b]

[a] State Key Laboratory of Coal Combustion, School of Energy and Power Engineering, Huazhong University of Science and Technology, Luoyu Road 1037, Wuhan, Hubei, 430074, PR China

[b] Joint International Center for CO_2 Capture and Storage (iCCS), Provincial Key Laboratory for Cost-effective Utilization of Fossil Aimed at Reducing Carbon-dioxide Emissions, College of Chemistry and Chemical Engineering, Hunan University, Lushannan Road 1, Changsha, Hunan, 410082, PR China

ARTICLE INFO

Article history:
Received 8 December 2017
Received in revised form
24 March 2018
Accepted 28 March 2018
Available online 28 March 2018

Keywords:
CO_2 capture
Oxy-fuel combustion
Process control
Dynamic exergy method
Dynamic simulation
Air separation unit

ABSTRACT

Cryogenic air separation unit (ASU) is considered as the currently available commercial oxygen production method for oxy-fuel combustion power plants; however, this method leads to significant energy penalty and economic cost. Real-time optimizing system operations during dynamic processes (such as flow rate change, oxygen product purity change, and flexible operation) are expected to achieve remarkable energy savings. Dynamic exergy provides a powerful indicator for real-time evaluating the system thermodynamic performance and quantifying the impact of a control strategy. In this work, some important transient exergy parameters of ASU systems under typical dynamic operating scenarios were first obtained through combining steady-state and dynamic process simulations. Next, control penalty and cost for internal control structures (layers and loops) were determined for the optimizations of control strategy and operation. Feedforward-feedback control structure and ASU-following control strategy are more suitable for ASU regulation and flexible operation, respectively, because more efficient thermodynamic performance is achieved during the investigated operating scenarios. The control structure, layer and loop play different roles in terms of energy behavior and require reasonable regulation to optimize energy behavior. This study provides an important insight into using control optimization aided by the dynamic exergy method to implement energy-efficient operations for industrial plants.

1. Introduction

To mitigate the greenhouse gas effects of the enormous CO_2 emissions from power plants on climate change, carbon capture, utilization and storage (CCUS) technology has been considered to be a very effective and promising route within a short term [1]. Oxy-fuel combustion, one of the competitive CCUS technologies, is currently ready for commercial demonstration. Oxy-fuel combustion uses the mixture of oxygen from an air separation unit (ASU) and recycled flue gas to replace air to combust with fuel, and then flue gas enriched by approximately 80–90 mol.% CO_2 is sent into a CO_2 compression and purification unit (CPU) to produce high-purity CO_2 for other industrial applications [2,3]. To meet the oxygen supply demand in oxy-fuel combustion, the ASU for oxygen production should possess the following traits [4–7]: (i) large O_2 production capacity with low product pressure (~1.5 bar), relatively low product purity (~95 vol%) and no necessity for other products; (ii) frequent and fast ramp demands; (iii) flexible operability; (vi) robust control performance; and most importantly, (v) low energy and cost penalties. Among the oxygen production approaches [8,9], cryogenic ASU appears to be the only available method currently for oxy-fuel combustion application [4,5]. However, cryogenic ASU demonstrates large energy penalty and high operating cost; these drawbacks would significantly deteriorate the thermodynamic and economic behaviors of oxy-fuel combustion power plants [10,11].

Many efforts have been made on new process design, process optimization, heat integration, control method and operating strategy to reduce the cost and energy consumption of the ASU. Several new ASU options adopted with above-ambient distillation have been proposed and compared based on the energy penalty, economic cost and operation reliability [5], and a sub-ambient heat

* Corresponding author.
E-mail addresses: klinsmannzhb@163.com, hzhao@mail.hust.edu.cn (H. Zhao).

https://doi.org/10.1016/j.energy.2018.03.154
0360-5442/

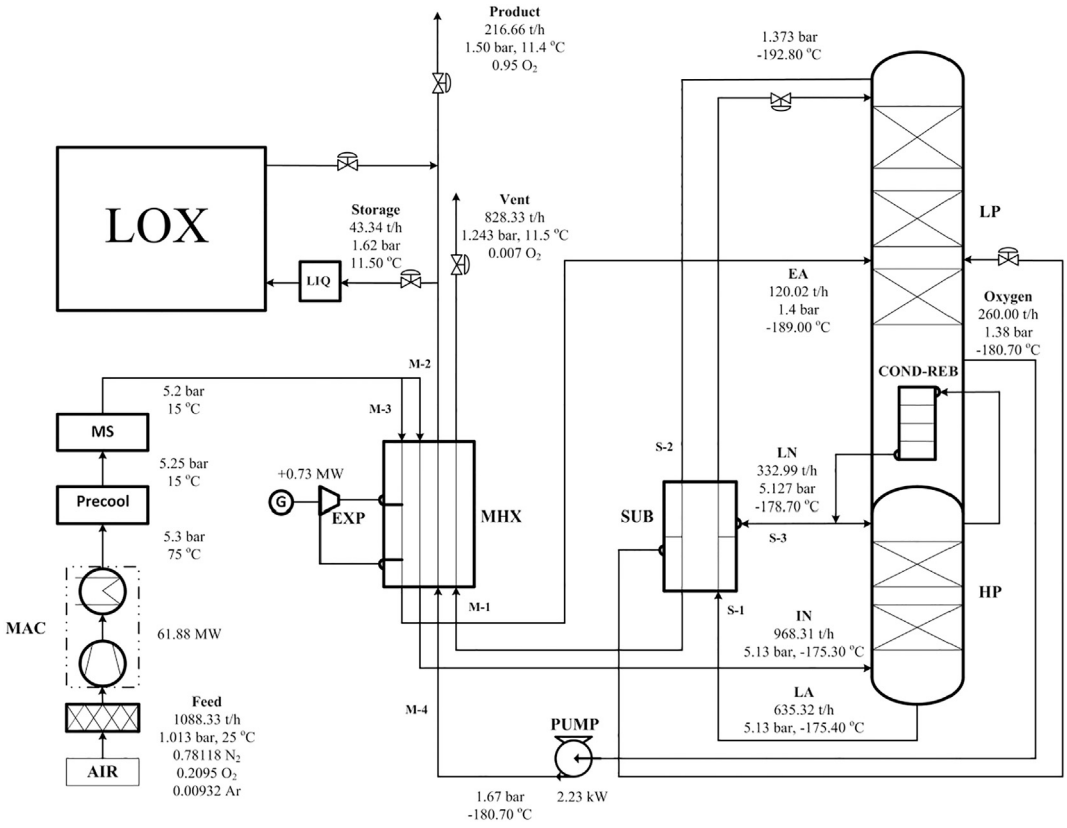

Fig. 1. Schematic of a dual-column based ASU with LOX in an oxy-fuel combustion power plant.

pump distillation with low energy consumption was designed as an alternative option [12]. Through applying the exergy assessment, some potential solutions to reduce the thermodynamic irreversibilities in the compression and distillation processes were reported to optimize the ASU performance [13]. Heat integration mainly focused on the effective utilization of compression duty from the ASU for other subsystems [4]. The energy penalty could reduce approximately 0.38% of the overall oxy-fuel combustion power plant when heat recovery was employed to preheat feed water sending into the boiler island [14], and a maximum of 0.12–0.22% more decrease could be further achieved if a mixed integer nonlinear programming model was applied to optimize this heat integration [15]. For control and operation, the strategies of phase CO_2 capture [16], energy storage operation [16], and peak and off-peak (POP) operation [17] were developed to increase system flexibility and reduce operating cost. Moreover, a control system [7] was designed to realize the preceding strategies and different integration patterns were tested to integrate the ASU with the oxy-fuel combustion boiler. Although these studies have provided useful ideas to achieve efficient and economic operations of the ASU in oxy-fuel combustion power plants, very limited studies focused on reducing power consumption of the ASU through control optimization.

In fact, the optimizations of control objective, control structure, and control performance could achieve energy conversation [18] and sustainable development [19]. The former two control aspects are always correlated by setting the minimization of energy consumption and economic cost as objective functions, selecting desirable control pairings, and establishing advanced control structure. Typically, self-optimizing control [20], model predictive control (MPC) [21] and real-time optimization (RTO) [22] are the primary methods to implement optimal control target and structure. Thus, control performance can be further optimized to enhance the thermodynamic and economic behaviors. An exergy-based method is an effective approach because exergy constructs the relationship between thermodynamics and process control. From the dynamic exergy equation, the system response time [23] was derived, the relative exergy array [24] was proposed, the eco-efficient exergy factor [25] was introduced, and the dynamic exergy plots [26] were used to identify and confirm the optimal control pairing. Nevertheless, this exergy-based method was based on the steady-state results and lacked clear evaluation indictors. To further improve the method, a new dynamic exergy method [27,28] was recently developed to achieve real-time evaluation of the thermodynamic performance of an oxy-fuel combustion boiler and a CPU, and the dynamic evaluation was based on the dynamic process simulation for these two systems [3,29,30]. The dynamic exergy methodology built a pathway to observe the dynamic exergy behavior and quantify the control impacts on system thermodynamic performance. A suitable control strategy and structure could be determined via the comparison of the total exergy destructions under different operating scenarios. Thus, remarkable energy savings for the ASU can be achieved when proper control system is adopted and optimized.

In this study, the dynamic exergy methodology was utilized to quantify the effects of internal structures (control layers and loops) in the control system on the ASU thermodynamic performance and then was used to determine the optimal control strategy. This paper is organized as follows. Section 2 gives a brief introduction to the studied ASU system in an oxy-fuel combustion power plant. In Section 3, the procedures and notes for the dynamic exergy method employed in the analyzed ASU are presented. In Section 4, comprehensive discussion to identify the control impacts on system energy behavior is illustrated, and the control optimization is

presented. Finally, conclusions are given in Section 5.

2. Air separation unit

Fig. 1 illustrates the process flow diagram of an ASU [7] in an oxy-fuel combustion power plant adopted and studied to optimize the ASU control performance. Pure atmospheric air depleted of particle impurities is compressed via a three-stage compressor with intercoolers (MAC), cooled by a precool unit (PU), treated with a molecular sieve (MS), and then split into two streams, before passing through the main heat exchanger (MHX) to heat product streams. One stream is directly sent into the high-pressure column (HP), and the other stream is expanded in the expander (EXP) to generate the required refrigeration capacity and enters the low-pressure column (LP). The nitrogen from the HP top is condensed against with the boiling oxygen in the condenser-reboiler (COND-REB), where one part acts as reflux stream for the HP, and the other part is depressurized via the subcooler (SUB) and throttle valve before being sent to the LP top. Liquid air from the HP bottom is also sent to the LP after depressurized by the SUB and throttle valve. The bottom oxygen product boosted by the liquid oxygen pump (PUMP) and waste nitrogen are heated through the MHX and then sent outside of the cold box. Last, one part of the oxygen product is supplied to the oxy-fuel combustion boiler, and the rest is stored in a liquid oxygen storage drum (LOX).

To satisfy operating demand and reduce energy penalty, the POP operating strategy [7,17] (Fig. 2) is employed here to integrate the ASU into the oxy-fuel combustion power plant. In this strategy, the ASU is oversized to 120% capacity and configured with LOX, and the oxy-fuel combustion boiler always operates at full load (100%). During off-peak time operation, 20% of the gaseous oxygen products are liquefied and stored in the LOX, while the rest are sent to the oxy-fuel combustion boiler. When at peak time, the ASU is turned down to the minimum load (60%), the gaseous oxygen product is stopped to be liquefied and stored into LOX, and gaseous oxygen vaporized from LOX (40%) enters the oxy-fuel combustion boiler. A control system [7], shown in Fig. 3, was designed to realize this operating strategy. In the control system, feedforward-feedback control structure is installed in the supervisory control layer to satisfy oxygen product quality and achieve the flexible operation. The former target is achieved via the control loops of oxygen product purity (CC_OXY), liquid oxygen level (LC_REB) and LP pressure (PC_LP), while the latter objective is attained by the "M_NOR", "M_ASU" and "M_LOX" strategies. "M_NOR" denotes the completion of normal operations, including load change and mode switching (air-fired mode and oxy-fired mode), and "M_ASU" and "M_LOX" aims to reach the POP operation. "M_ASU", i.e., the ASU-following control strategy, defines an oxygen supplying rate from LOX beforehand while tracking and maintaining the total oxygen flow rate required for oxy-fuel boiler via adjustment of the set-point of FC_LGOX. Operated in an opposite manner, "M_LOX"

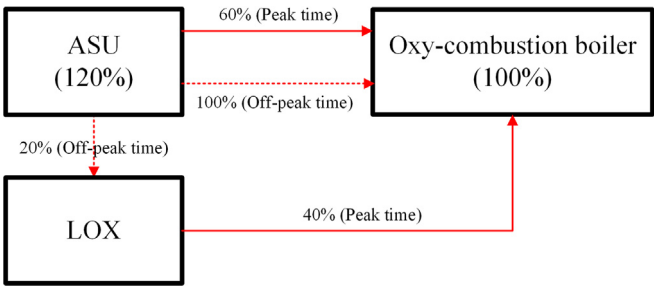

Fig. 2. Simplified explanation of the POP operating strategy.

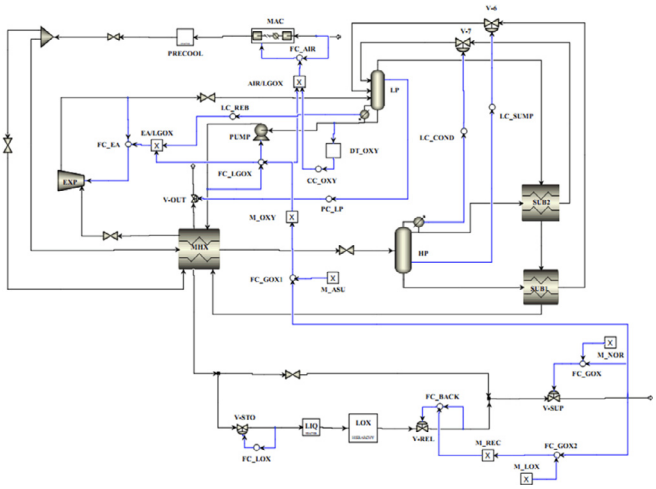

Fig. 3. Dynamic model for the ASU with feedforward-feedback control structure.

(also called LOX-following control strategy) is achieved by providing an oxygen supply rate from the ASU in advance while the set-point of FC_BACK is regulated to satisfy the total oxygen demand from oxy-fuel combustion boiler. The total compression power consumption was found to decrease by approximately 32.85% [7].

3. Applying the dynamic exergy method to ASU

As shown in Fig. 4, the dynamic exergy method proposed by us [27,28] is adopted here to evaluate and optimize the control behavior. As the first step, a steady-state model is first established and validated against with the plant design data, and then the model is converted into the dynamic model. Here, the closed-loop control system is configured to conduct dynamic simulations when the various operating commands are applied. From the dynamic behavior, the real-time thermodynamic parameters, consisting of flow rate (m), pressure (P), temperature (T), power consumption (W) and composition (c), are obtained to calculate the exergy parameters under the supervision of the closed-loop control system. Moreover, the thermodynamic parameters for the case that the plant runs without any control intervention are also obtained when the identical operating commands are input into the steady-state simulation. Finally, these closed-loop and open-loop thermodynamic information are used as the inputs in the exergy calculation program. The physical exergy (E^{PH}), chemical exergy (E^{CH}), fuel exergy (E_F), product exergy (E_P), exergy destruction (E_D), and exergy efficiency (η) [11,31,32] are introduced to evaluate the system exergy performance. In step 2, based on the determined dynamic exergy plots, the dynamic exergy property is displayed directly, the energy consumption for the operating scenario is calculated, the sensitivity of the operating parameter is identified, the control penalty and the control cost are quantified, and the control strategy is compared and selected. These five aspects, referred from our previous studies [27,28], can be used to determine the optimal control structure and performance.

Specifically, the detailed procedures to implement dynamic exergy analysis for the studied ASU are presented. As discussed in our previous study [7], the steady-state model was established based on the following assumptions: (1) pure air components (78.118% N_2, 20.95% O_2 and 0.932% Ar) were considered to simplify the process model, (2) a combination of the HP with condenser and the LP with the reboiler was employed to represent two distillation columns and COND-REB, and (3) the design specification and

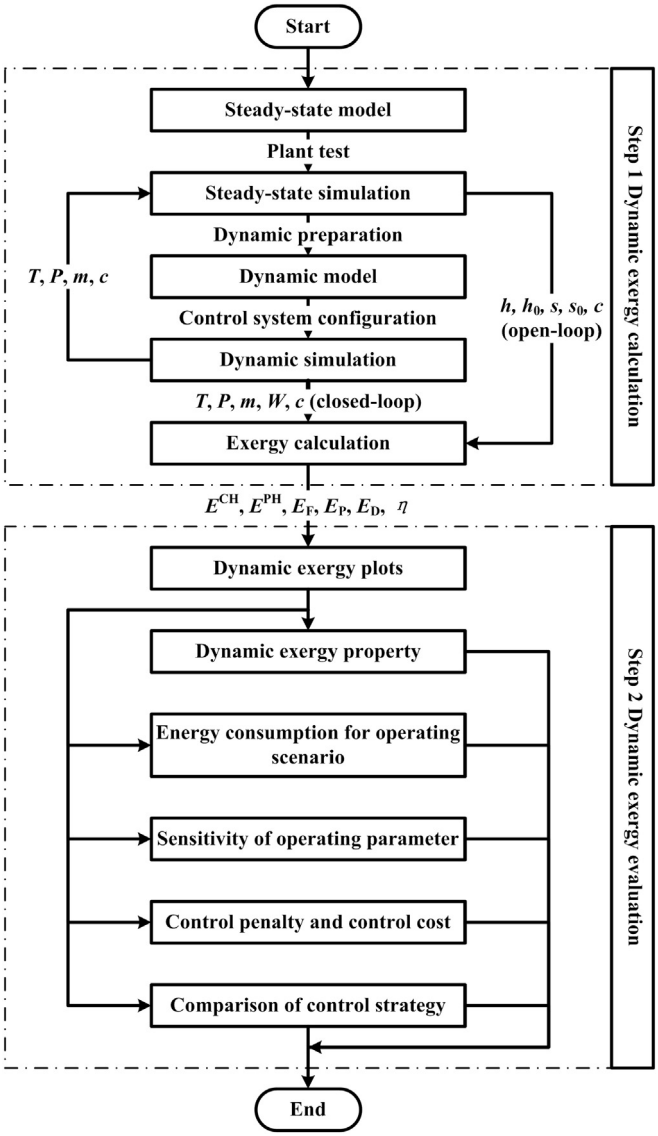

Fig. 4. Systematic procedures for the execution of the dynamic exergy method.

calculator modules were used to ensure full heat integration and oxygen product demands. Moreover, oxygen liquefaction and vaporization processes are simplified in the developed model without considering the detailed real conditions such as process type, device type, and refrigeration recovery, etc. Next, the dynamic model was built after the accomplishment of the dynamic preparations by choosing the pressure-driven method, setting the connections between two-unit devices and importing the geometric sizes of the MHX, SUB, COND-REB, HP and LP. As illustrated in Fig. 3, a closed-loop control system was configured to conduct dynamic simulations under the conditions of load change, oxygen product purity change and POP operation. Hence, the real-time thermodynamic data under control systems with different structures and strategies during the preceding three operating scenarios can be obtained. Finally, based on the reference environmental state, the exergy parameters to assess the ASU performance are calculated. The energy consumptions from liquefaction and vaporization are considered as the parts of fuel exergy and their calculations are determined from the correlation of energy consumption from ASU process and the varied amounts of liquefied oxygen and re-vaporized oxygen during different operating scenarios. It is assumed that the energy consumptions from liquefaction and vaporization are respectively set as 1.4 times and 0.6 times of that from ASU, if all the produced gaseous oxygen from ASU is used for liquefaction and liquified oxygen is used for vaporization (using steam as the heating medium). In the initial state (120% oxygen products with 100% gaseous oxygen and 20% liquid oxygen), the fuel exergy includes the exergy of atmosphere air (E_{air}; 806.89 kW, 1.049%), the exergy of liquid oxygen supplied to oxy-fuel boiler ($E_{o,s}$; 0 kW, 0%), the power consumptions from MAC (E_{mac}; 61876.30 kW, 80.408%), liquefaction (E_{liq}; 14267.85 kW, 18.541%), PUMP (E_{pump}; 2.18 kW, 0.003%) and vaporization (E_{vap}; 0 kW, 0%), while the product exergy consists of the exergy of gaseous oxygen product ($E_{o,g}$; 8548.77 kW, 45.69%), the exergy of liquid oxygen product ($E_{o,l}$; 9432.06 kW, 50.41%) and the power produced from EXP (E_{exp}; 730.54 kW, 7.87%). In such a manner, the exergy destruction and exergy efficiency are determined as 58241.86 kW and 24.32%, respectively. Therefore, the dynamic exergy plots are formed by calculating the exergy parameters at all operating time points.

Dynamic exergy property denotes the real-time exergy behavior displayed directly in the dynamic exergy plots. The energy performance for operating scenario (α_i) is determined from Eq. (1) by counting the areas under dynamic exergy curves. The energy inputs (α_F), energy outputs (α_P) and energy consumptions (α_D) for three operating cases during the selected time period are the areas under the dynamic fuel exergy, product exergy and exergy destruction curves, respectively. This parameter describes the energy performance caused by an operating command during a time period. As presented in Eq. (2), the energy utilization ratio (λ), defined as the ratio of the total energy outputs to the total energy inputs, is introduced to represent the extent of energy utilization for the operating case and the control system. A control system would be more energy-efficient when this parameter for one control system is larger than that of another control system; in the opposite situation, the control system would cause a higher energy penalty. Sensitivity factor (β) formulated as Eq. (3) is introduced to identify the sensitivity level of operating parameter on system operation. The larger sensitive factor would lead to the greater fluctuation during system operation at the situation that the corresponding operating parameter changes.

$$\alpha_i = \int_{t_0}^{t_1} E_i(t)dt \tag{1}$$

$$\lambda = \frac{\alpha_P}{\alpha_F} \tag{2}$$

$$\beta = \left| \left(\frac{d\alpha_D}{\alpha_{D,0}} \right) \Big/ \left(\frac{du}{u_0} \right) \right| \tag{3}$$

where α is energy (kW·h) including α_F, α_P and α_D, t is time point, subscripts "0" and "1" stand for the initial and final operating states, and i means the types of exergy parameters (i.e. E_F, E_P, and E_D); λ is energy utilization ratio, subscripts "F" and "P" represent the fuel and product; β is a non-dimensional number, $d\alpha_D$ is the amount of energy consumption that generated during the time period from giving command to reaching the final steady-state, $\alpha_{D,0}$ mean the produced energy consumption if the initial operating condition lasts for the above time period, and u is the variable used to complete the operating command, and u_0 is the initial value of u.

However, because of the convergence problem that occurs in the dynamic simulation of ASU, the direct calculations of control penalty and control cost based on open-loop control are infeasible

because dynamic exergy plots under open-loop control for ASU are unavailable. To solve this issue, control penalty ($\Delta\alpha$), defined as the difference of energy consumption between two different control systems, is introduced to represent the impacts of control structure, layers and loops on system performance. As shown in Eq. (4), control penalty is calculated by acquiring the energy consumption under all control systems simultaneously. Therefore, the inherent energy performance for control layers and loops in the control system can be uncovered to identify their contributions to system thermodynamic characteristics and to optimize control structures with the aim of reducing energy consumption. Moreover, Eq. (4) can also be used for the comparison of control strategies (δ) via obtaining the difference of energy consumption between two control strategies. From Eq. (5), control cost (k) is the absolute value of the ratio of the total fuel impact to the total product impact. In fact, the control cost quantifies the demand of the control effort to achieve the desirable product quality when the fuel input is no longer equal to the specified value. More attention should be paid to an operating parameter if the corresponding control cost is larger. For internal control structures, the value of control cost can also be used to reveal the important extent of control layers and loops during a certain operating scenario.

$$\Delta\alpha(\delta) = \alpha_{D,A} - \alpha_{D,B} \tag{4}$$

$$k = \left| \frac{\alpha_{F\_closed} - \alpha_{F\_j}}{\alpha_{P\_closed} - \alpha_{P\_j}} \right| \tag{5}$$

where, $\Delta\alpha$ or δ is the difference of energy consumption, subscripts "A" and "B" are two different control configurations or strategies, k is control cost, and i means control systems configured with different control layers and loops.

4. Results and discussion

4.1. Dynamic exergy property

4.1.1. Flow rate change case

Fig. 5 shows the dynamic exergy properties of the ASU during the flow rate change process where oxygen flow rate ramps down 20% from the initial state with a rate of 2%/min. Six control structures are considered at the operating scenario. Generally, fuel exergy decreases because E_{air}, E_{mac}, E_{liq} and E_{pump} are all decreased, while product exergy decreases via the decrements of the flow rates of the expanded air and oxygen products. Unfortunately, the ASU cannot operate when the liquid oxygen level control loop is not installed. This collapse of operation is ascribed to the failure of thermodynamic pairing between vaporization and condensation in the condenser-reboiler. Therefore, the former 30 min are chosen for the regulatory control layer case (Fig. 5(a)).

Control cases (b), (c), and (d) are identical in terms of fuel exergy because the presence of the oxygen product purity control loop contributes to the same values of the exergy parameters. Because of the larger decrement of E_{mac}, the fuel exergy of case (e) is lower than that of case (f). The difference between cases (f) and (a) is ascribed to the control actions from supervisory control layer in the former case. That control layer causes the different amounts of atmosphere air and power consumption from the three-stage compressor with intercoolers. With respect to product exergy, case (c) is larger than case (b) because the smaller decrements of E_{exp} and $E_{o,\,l}$ are observed in the former control structure. The product exergy of case (d) is larger than that of case (c) because the feedforward control signal from CC_OXY makes oxygen product purity be closer to the target in case (a). The difference between

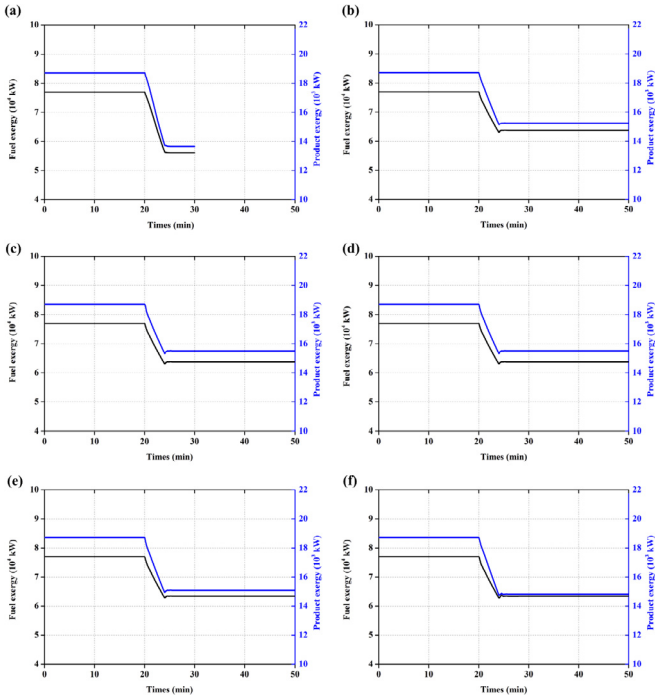

Fig. 5. Dynamic exergy properties for the ASU configured with six control structures during flow rate change process: (a) regulatory control layer (**RCL**), (b) oxygen product purity control (**OXY**), (c) the coupling of oxygen product purity with liquid oxygen level controls (**OL**), (d) supervisory control layer (**SCL**), (e) feedforward-feedback control (**FF**), and (f) feedback control (**F**).

cases (b) and (e) is derived from the real-time regulations of CC_OXY and LC_REB on the expander operation. Because the presence of feedforward compensation leads to the different oxygen product purity, the product exergies of cases (e) and (f) are slightly different. The oxygen product purity remaining at the set-point by CC_OXY and the higher power produced from expander make the product exergy of case (f) different from that of case (a). As determined from the dynamic behavior of fuel and product exergies, time-varied exergy destruction and exergy efficiency were obtained (for simplicity, the results are not shown here). In the feedforward-feedback control case, the decrease of exergy destruction occurs because the decrement of fuel exergy (−13528.92 kW) is larger than that of product exergy (−3631.32 kW), while the change of exergy efficiency occurs because of the relationship between the extent of variations of the fuel and product exergies.

4.1.2. Oxygen product purity change case

The dynamic exergy property is shown in Fig. 6, illustrating that the oxygen product purity increases linearly from 95 mol.% to 99.75 mol.% while oxygen product flows are maintained at the initial state. All the exergy parameters increase under feedforward-feedback control system. For fuel exergy, this finding is ascribed to the fact that E_{pump} decreases by approximately 0.27% while E_{air}, E_{liq} and E_{mac} increase by approximately 0.40%, 1.82% and 1.77%, respectively. Because of the regulations of oxygen product purity and liquid oxygen level controls, $E_{o,\,g}$ and $E_{o,\,l}$ are increased (+2.76% and 0.43%) while E_{exp} decreases (−2.55%). The increment of fuel exergy (+1356.70 kW) is larger than that of product exergy (+258.31 kW), whereas the amplitude of the variation for fuel exergy (+1.76%) is larger than that of product exergy (+1.89%). Hence, exergy destruction increases while exergy efficiency decreases. In addition, the dynamic exergy behavior for **FF** is different

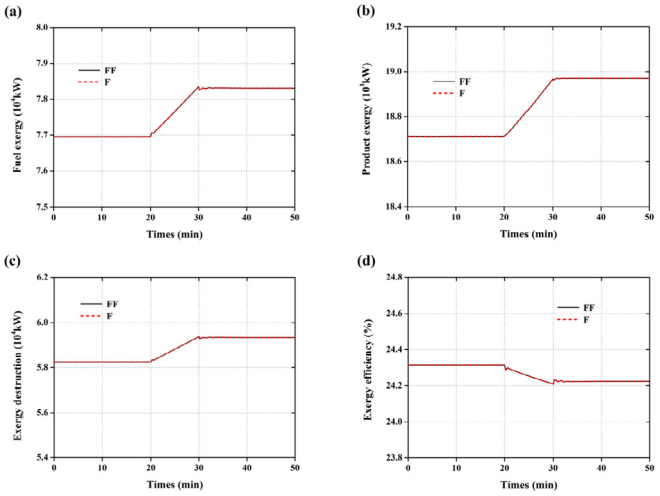

Fig. 6. Dynamic exergy property for the ASU during the oxygen product purity change process: (a) fuel exergy, (b) product exergy, (c) exergy destruction, and (d) exergy efficiency.

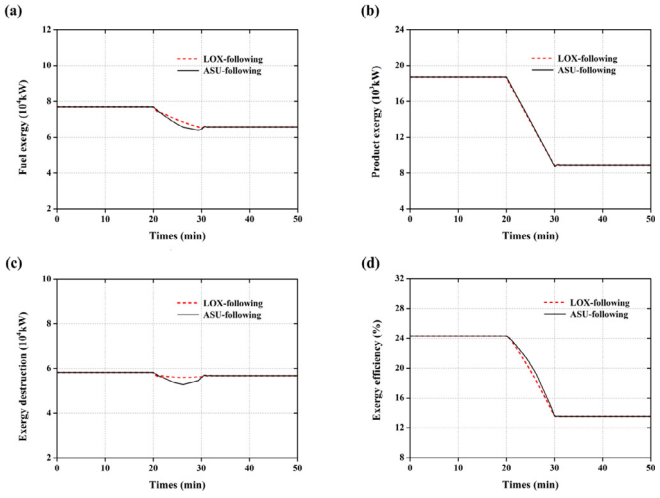

Fig. 7. Dynamic exergy property for the ASU during POP operation: (a) fuel exergy, (b) product exergy, (c) exergy destruction, and (d) exergy efficiency.

from that of **F** because feedforward function contributes to slight differences for atmosphere air flow rate, power consumption from compressor, and oxygen product purity.

4.1.3. POP operation

Dynamic exergy responses of ASU under POP operation are shown in Fig. 7. All the exergy parameters decrease for both the LOX-following and ASU-following operating strategies. For the LOX-following strategy, the variation of fuel exergy is derived from the variations of E_{air}, $E_{o,\,s}$, E_{mac}, E_{liq}, E_{vap} and E_{pump}, especially the significant decreases of E_{mac} and E_{liq} while the increments of E_{vap} and $E_{o,\,s}$. In terms of product exergy, all the components get the decrements. The reason for this behavior is that the expander operation is regulated to satisfy the liquid oxygen level demand, oxygen product quality should be maintained to meet with the oxygen supply demand, and oxygen product is gradually stopped to be liquefied and stored into the LOX. The amount and amplitude of the variation for fuel exergy (−11355.06 kW, −14.75%) are larger than those of product exergy (−9846.26 kW, −52.62%), leading to the variations of exergy destruction and exergy efficiency. As discussed in our previous study [7], the different exergy behavior for LOX-following and ASU-following results from where the control signal for the oxygen product flow rate is sent.

4.2. Energy consumption of operation and sensitivity factor

Energy consumptions for three operating cases are summarized in Table 1. The highest energy utilization ratio for oxygen product purity case indicates this process realizes the most effective usage of energy. During an identical operating condition, the role played by feedforward compensation results in little difference in the energy performance between feedforward-feedback control and feedback control. Moreover, feedforward compensation could enhance the energy utilizations for flow rate and POP cases while slightly weaken the energy behavior for oxygen product purity case. The thermodynamic performance for ASU-following strategy is more efficient than that of LOX-following strategy. Although the former strategy leads to higher energy consumption from the compressor, it makes the oxygen product purity more close to the set point and less oxygen flow rate supplied to the oxy-fuel combustion boiler. In such a way, the amount of exergy decrease caused by oxygen product purity and oxygen flow rate supplied from LOX is larger than that of exergy increment resulted from compression power. The sensitivity factors for flow rate and oxygen product purity change cases are determined as 4.41 and 101.33, respectively. In other words, the variation of the oxygen product purity causes the larger energy consumption than that of the flow rate, indicating that the ASU operation is more sensitive to the change of oxygen product purity.

4.3. Control penalty and control cost

From Table 2, the control penalty for closed-loop control structure is determined as 738.05 kW h, which represents the necessary energy consumption required to achieve oxygen product quality and ensure robust operation. The main energy penalty is not caused by the control system (2.65%, supervisory control layer occupies 2.60% and regulatory control layer accounts for 0.05%) but originates from the operation without the control system (97.34%). This penalty implies that the system self-characteristic and limitation from the unit device rather than the control system are the main sources of thermodynamic inefficiency. In the control system,

Table 1
Energy inputs, outputs and utilization ratios for three operating cases.

Case, kW·h	FF			F		
	α_F	α_P	λ^a	α_F	α_P	λ^a
Flow rate change	57753.28	13885.43	24.04	57756.54	13770.19	23.84
Oxygen product purity change	64697.30	15699.33	24.27	64697.30	15699.34	24.27
POP operation: LOX-following	53650.36	11477.60	19.39	53660.11	11478.73	19.39
POP operation: ASU-following	53725.35	11488.66	19.50	53727.73	11489.21	19.50

[a] Calculated from Eq. (2), with the difference for **FF** and **F** being quite small during an identical operating case.

Table 2
Energy consumptions for different control configurations (kW·h).

Control type[a]	α_D	Control type[b]	$\Delta\alpha$
FF	27753.10	LC_REB	−27.81
OXY	27765.74	CC_OXY	750.69
OL	27737.93	Feedforward-feedback	−0.03
SCL	27737.90	Regulatory control layer	15.20
RCL	27030.25	Supervisory control layer	722.85
Open-loop	27015.05	Closed-loop control structure	738.05

[a] ASU configured with different control structures or systems.
[b] Different control structures, layers and loops.

the supervisory control layer consumes approximately 97.94% of the total energy consumption, with the rest originating from the regulatory control layer. This phenomenon is attributed to the different roles played: the regulatory control layer maintains steady operation and resists local disturbance, whereas the supervisory control layer pushes the operating parameters close to their targets and optimizes the operation. Thus, a small control penalty is required for the regulatory control layer while more energy consumption is required in the supervisory control layer. CC_OXY and LC_REB in the supervisory control layer are used to maintain oxygen product purity and liquid oxygen level via the control actions on the atmosphere air flow rate and the EXP, respectively. LC_REB and feedforward-feedback compensation save energy while CC_OXY consumes energy. Because the speed of EXP is turned down to bring the high liquid oxygen level back to the set-point, energy savings can be realized from LC_REB. The energy penalty for CC_OXY is the maximum because it aims to maintain oxygen product purity at approximately 95mol.%. More power consumption is required when the oxygen product purity is lower than its set-point because a larger amount of atmosphere air is required to achieve the control target. In nature, the energy penalty for CC_OXY arises from the variation of stream composition (i.e., the change of chemical exergy), and that of LC_REB and feedforward-feedback compensation results from the variation of stream flow rate (i.e., the change of physical exergy).

From Table 3, the costs for the control structure, layers and loops are different because their targets and functions are different. The costs for regulatory and supervisory control layers are 0.714 and 5.252, respectively, revealing that larger control effort is required in the supervisory control layer than that of the regulatory control layer to realize the control objectives. The costs for control loops in supervisory control layer are ranked as: CC_OXY > LC_REB> feedforward-feedback compensation, which reflect the difficult extent of implementing the corresponding control loop. In addition, it is found that the cost for closed-loop control structure is the sum of the costs for the corresponding control layers, and the cost for supervisory control layer is the sum of the costs for the corresponding control loops in this layer.

4.4. Comparison of control strategies

Table 4 lists the energy consumptions for feedforward-feedback control and feedback control during three operating scenarios. The former control consumes less energy than that of the latter one for all the cases, which is attributed to that feedforward-feedback compensation reduces the energy consumption from the compressor where the amount of atmosphere air is decreased. Two control systems contribute to almost identical energy performance during oxygen product purity change process. Additionally, energy consumption for ASU using the ASU-following operating strategy is lower than that of using the LOX-following operating strategy (i.e. −275.50 kW h for feedforward-feedback control and −275.45 kW h for feedback control), because the deviation of the oxygen product purity using the first strategy is lower and the oxygen supplying flow rate is smaller than that of using the second strategy.

Table 4
Comparison of different control strategies and control systems.

Case, kW·h	FF	F	δ
Flow rate change	50963.58	50966.39	2.81
Oxygen product purity change	48997.968	48997.969	0.001
POP operation: LOX-following	47703.20	47711.81	8.60
POP operation: ASU-following	47427.71	47436.35	8.65

5. Conclusions

The dynamic exergy method was used to improve the thermodynamic and economic performance of an oxy-fuel combustion power plant integrated with a cryogenic air separation unit (ASU) because the ASU has high energy and economic costs. The ASU can achieve energy-efficient operation through control optimization based on the dynamic exergy calculation and evaluation. Indeed, this dynamic exergy methodology can be used to observe the dynamic exergy property, calculate the energy consumption for operating scenario, analyze the sensitivity of operating parameter, determine the control penalty and control cost, and compare the control strategy. It was found that the dynamic exergy property is related to the analyzed operating cases, and the most effective energy utilization occurs in oxygen product purity change case when compared to other operating scenarios. The control system requires 738.05 kW h energy penalty to maintain stable and robust operation, and the main thermodynamic inefficiency originates from the system intrinsic characteristics (i.e., plant structure and equipment performance). Supervisory control layer requires greater energy consumption than that of the regulatory control layer, and the oxygen product purity control loop contributes to the primary energy penalty in the supervisory control layer. The ASU-following control strategy is a more suitable strategy because its energy consumption is lower than that in the LOX-following control strategy. It was found that the sensitivity factor for the oxygen product purity change case is the maximum, indicating that the variation of oxygen product purity has the most significant effect on system operation. The energy penalty of control system is required to maintain stable and safety operation, and different internal

Table 3
Control costs for the control loops and control layers during the flow rate change process.

Control type	α_{F_closed}	α_{F_i}	α_{P_closed}	α_{P_i}	k
LC_REB					0.768
CC_OXY					3.752
Feedforward-Feedback	36611.84	36649.71	8858.74	8911.78	0.7140
Regulatory control layer	36611.84	36649.71	8588.74	8911.81	0.7136
Supervisory control layer	36611.84	35718.99	8588.74	8688.74	5.252
Closed-loop control structure					5.966

control structures (layers and loops) in the control system exhibit different energy performances. The control cost of the closed-loop control system is the sum of the control costs of all control layers, and the sum of the control costs of all control loops in a control layer is the control cost for that control layer. Feedforward-feedback control was selected for the studied ASU because it achieved energy-efficient operation. In summary, this study provides useful information for engineers and other applications to achieve desirable operation through control optimization.

Acknowledgements

This work is supported by “National Key R&D Program of China (2016YFB0600801)”, “National Natural Science Foundation of China (51390494 and 51522603)” and “Fundamental Research Funds for the Central Universities (531107050907)”. Special thanks should be given to Mr. Jun Cao from Sichuan Air Separation Plant (Group) Co., Ltd for providing some useful information on this study.

Notation

Symbols

c	composition
d	differential
E	exergy
h	unit enthalpy, kJ/kmol
k	control cost
m	flow rate
P	pressure
s	unit entropy, $kJ \cdot kmol^{-1} \cdot K^{-1}$
t	time point
T	temperature
W	power consumption

Subscripts

0	reference environment state/initial operating state
1	final operating state
A, B	different control systems or strategies
D	destruction
F	fuel
i	exergy type
j	control type
P	product

Superscripts

CH	chemical
PH	physical

Greek symbols

α	energy (kW·h)
β	sensitivity of operating parameter, a non-dimensional number
Δ	difference
λ	energy utilization ratio
δ	energy difference
η	exergy efficiency

Abbreviations

ASU	air separation unit
CCUS	carbon capture, utilization and storage
CPU	CO_2 compression and purification unit
CC_OXY	oxygen product purity control loop
COND-REB	condenser-reboiler
EXP	expander
F	feedback control
FC_BACK	flow rate control loop(oxygen supply from LOX)
FC_LGOX	flow rate control loop(liquid oxygen product from LP)
FF	feedforward-feedback control
HP	high pressure column
LC_REB	liquid oxygen level control loop
LOX	liquid oxygen storage drum
LP	low pressure column
MAC	main air compressor
MHX	main heat exchanger
MPC	model predictive control
MS	molecular sieve
M_ASU	ASU-following control strategy
M_LOX	LOX-following control strategy
M_NOR	normal operating strategy
OXY	oxygen product purity control
OL	the coupling of oxygen product purity with liquid oxygen level controls
PC_LP	LP operating pressure control loop
POP	peak and off-peak time operation
PU	purification unit
PUMP	liquid oxygen product pump
RCL	regulatory control layer
REA	relative exergy array
REDA	relative exergy destruction array
RGA	relative gain array
RTO	real-time optimization
SCL	supervisory control layer
SUB	subcooler

References

[1] Boot-Handford ME, Abanades JC, Anthony EJ, Blunt MJ, Brandani S, Mac Dowell N, et al. Carbon capture and storage update. Energ Environ Sci 2014;7:130–89.
[2] Jin B, Zhao H, Zheng C. Dynamic simulation for mode switching strategy in a conceptual 600MWe oxy-combustion pulverized-coal-fired boiler. Fuel 2014;137:135–44.
[3] Jin B, Zhao H, Zheng C. Dynamic modeling and control for pulverized-coal-fired oxy-combustion boiler island. Int J Greenh Gas Control 2014;30:97–117.
[4] Darde A, Prabhakar R, Tranier J-P, Perrin N. Air separation and flue gas compression and purification units for oxy-coal combustion systems. Energy Proc 2009;1:527–34.
[5] Higginbotham P, White V, Fogash K, Guvelioglu G. Oxygen supply for oxyfuel CO_2 capture. Int J Greenh Gas Control 2011;5:S194–203.
[6] Tranier J-P, Dubettier R, Darde A, Perrin N. Air Separation, flue gas compression and purification units for oxy-coal combustion systems. Energy Proc 2011;4:966–71.
[7] Jin B, Su M, Zhao H, Zheng C. Plantwide control and operating strategy for air separation unit in oxy-combustion power plants. Energy Convers Manag 2015;106:782–92.
[8] Smith A, Klosek J. A review of air separation technologies and their integration with energy conversion processes. Fuel Process Technol 2001;70:115–34.
[9] Deng Z, Jin B, Zhao Y, Gao H, Huang Y, Luo X, et al. Process simulation and thermodynamic evaluation for chemical looping air separation using fluidized bed reactors. Energy Convers Manag 2018;160:289–301.
[10] Xiong J, Zhao H, Chen M, Zheng C. Simulation study of an 800 MWe oxy-combustion pulverized-coal-fired power plant. Energy Fuels 2011;25:2405–15.
[11] Xiong J, Zhao H, Zheng C. Exergy analysis of a 600 MWe oxy-combustion pulverized-coal-fired power plant. Energy Fuels 2011;25:3854–64.
[12] Fu C, Gundersen T. Recuperative vapor recompression heat pumps in cryogenic air separation processes. Energy 2013;59:708–18.
[13] Fu C, Gundersen T. Using exergy analysis to reduce power consumption in air separation units for oxy-combustion processes. Energy 2012;44:60–8.
[14] Fu C, Gundersen T. Integrating the compression heat in oxy-combustion power plants with CO_2 capture. Chem Eng Trans 2012;29:781–6.
[15] Fu C, Anantharaman R, Gundersen T. Optimal integration of compression heat with regenerative steam Rankine cycles in oxy-combustion coal based power plants. Energy 2015;84:612–22.
[16] Perrin N, Dubettier R, Lockwood F, Tranier J, Bourthy-Weber C, Devaux M. Oxycombustion for carbon capture on coal power plants and industrial processes: advantages, innovative solutions and key projects. Energy Proc 2013;37:1389–404.
[17] Hu Y, Li X, Li H, Yan J. Peak and off-peak operations of the air separation unit

in oxy-coal combustion power generation systems. Appl Energ 2013;112:747–54.
[18] Shinskey F. Energy conservation through control. New York: Academic Press; 1987.
[19] Daoutidis P, Zachar M, Jogwar SS. Sustainability and process control: a survey and perspective. J Process Contr 2016;44:184–206.
[20] Skogestad S. Plantwide control: the search for the self-optimizing control structure. J Process Contr 2000;10:487–507.
[21] Qin SJ, Badgwell TA. A survey of industrial model predictive control technology. Control Eng Pract 2003;11:733–64.
[22] Darby ML, Nikolaou M, Jones J, Nicholson DRTO. An overview and assessment of current practice. J Process Contr 2011;21:874–84.
[23] Luyben WL, Tyreus BD, Luyben ML. Plantwide process control. New York: McGraw-Hill; 1998.
[24] Montelongo-Luna JM, Svrcek WY, Young BR. The relative exergy array—a new measure for interactions in process design and control. Can J Chem Eng 2011;89:545–9.
[25] Munir M, Yu W, Young B. Plant-wide control: eco-efficiency and control loop configuration. ISA T 2013;52:162–9.
[26] Munir MT, Yu W, Young BR. Dynamic exergy plots using exergy factor. Trans Control Mech Syst 2012;1:13–9.
[27] Jin B, Zhao H, Zheng C. Dynamic exergy method and its application for CO_2 compression and purification unit in oxy-combustion power plants. Chem Eng Sci 2016;144:336–45.
[28] Jin B, Zhao H, Zheng C, Liang Z. Dynamic exergy method for evaluating the control and operation of oxy-combustion boiler island systems. Environ Sci Technol 2017;51:725–32.
[29] Jin B, Zhao H, Zheng C. Optimization and control for CO_2 compression and purification unit in oxy-combustion power plants. Energy 2015;83:416–30.
[30] Jin B, Zhao H, Zheng C. Dynamic Simulation and Control Design for pulverized-coal-fired oxy-combustion power plants. Clean coal technology and sustainable development. Springer; 2016. p. 325–33.
[31] Bejan A, Tsatsaronis G, Moran M. Thermal design & optimization. New York: John Wiley & Sons; 1996.
[32] Jin B, Zhao H, Zou C, Zheng C. Comprehensive investigation of process characteristics for oxy-steam combustion power plants. Energy Convers Manag 2015;99:92–101.